Study of the Nature and Mechanism of the Rhombohedral-to-Cubic Phase Transition in α-AlF₃ with Molecular Dynamics Simulations

Santanu Chaudhuri,[†,#] Peter J. Chupas,[†,⊥] Mark Wilson,[‡] Paul Madden,[§] and Clare P. Grey*,[†]

Department of Chemistry, SUNY Stony Brook, Stony Brook, New York 11794, Department of Chemistry, University College London, 20 Gordon Street, London WC1H 0AJ, United Kingdom, and Physical and Theoretical Chemistry Laboratory, Oxford University, South Parks Road, Oxford OX1 3QZ, United Kingdom

α-AlF₃, which adopts a rhombohedrally distorted form of the ReO₃ structure at room temperature, undergoes a phase transition to the cubic ReO₃ structure at 466 °C. The phase transition has been studied using molecular dynamics (MD) simulations performed with a polarizable ion model (PIM). The results are compared to information obtained from experimental diffraction data, and analogies to the tilting schemes of the structurally related perovskite phases are made. The cubic phase can be distinguished from the rhombohedral phase by following the Al–F–Al bond angles that describe the tilting of the AlF₆ corner sharing octahedra as a function of temperature. The Al–F–Al chains are still bent in the so-called cubic phase, but the direction of tilting of the AlF₆ octahedra varies continuously during the MD run, so that the time-averaged symmetry of the system is nearly cubic. The motion of the octahedra primarily involves a 360° rotation of the vector that describes the displacement of the F atom from its ideal position in a linear Al–F–Al chain. It is this 360° motion that distinguishes the cubic from the rhombohedral phase. The high-temperature phase is also associated with increased vibrations of the Al–F–Al chains. The results provide an explanation for the large thermal parameters observed experimentally for fluorine (in structures refined from diffraction data) above the phase transition. The simulation results suggest the possible existence of a third (orthorhombic) form of α-AlF₃, which is energetically very similar to the rhombohedral phase at room temperature but differs in its octahedral tilting scheme.

1. Introduction

Aluminum fluorides have been the subject of much recent research, motivated primarily by the catalytic activity of these materials in acid-catalyzed reactions[1,2] and reactions involving F/Cl exchange in halocarbons.[3] The latter reactions represent possible methods for synthesizing hydrofluorocarbons (HFCs), the alternatives to the less-environmentally friendly chlorofluorocarbons. The structural chemistry of aluminum fluoride is extremely diverse, and a wide range of different phases have now been prepared.[4] The thermodynamically stable form of aluminum fluoride α-AlF₃ adopts a rhombohedrally distorted form of the ReO₃ structure at room temperature (Figure 1) but undergoes a phase transition to the cubic ReO₃ structure at 466 °C.[5] The material is a poor catalyst for fluorine/chlorine exchange reactions.[3] In contrast, the form of α-AlF₃ that grows in-situ during halogen exchange reactions[6,7] with hydrochlorofluorocarbons (HCFCs) and HFCs over γ-Al₂O₃ is catalytically active. In previous structural studies,[6] we showed that the two forms of α-AlF₃ differ in the extent and temperature dependence of the rhombohedral distortions of these materials.

The temperature-dependent behavior of α-AlF₃ is similar to that of a variety of structurally related perovskites, where a transition from a distorted (or tilted) perovskite, to the cubic phase, can sometimes occur at elevated temperatures. For some space groups, this phase transition is associated with the loss of ferro-electric or -elastic behavior. For example, the double perovskite Na₃AlF₆ (cryolite) undergoes a phase transition from a monoclinic to an orthorhombic phase at 612 °C.[8] Another extensively studied mineral, the perovskite NaMgF₃, adopts an orthorhombic phase (*Pnma*) at room temperature but undergoes a phase transition to a high-temperature cubic phase at 767 °C. The distortions in this material have been studied by using neutron diffraction and molecular dynamics (MD) simulations[9] to understand nature of thermal vibrations responsible for the cubic structure. It also undergoes a phase transition[10] to a triclinic and then finally to a cubic phase with increased K for Na substitution. A major driving force for the distortions in these perovskites arises from a mismatch in the size of the A cation and the size of the hole formed by the corner sharing BX₆ octahedra. The type of distortion (i.e., the tilting system[11–14]) can be predicted for many systems by the program SPuDS[15] (Structure Prediction Diagnostic Software) developed by Woodward et al., which uses the bond-valence model of Brown et al[16] to determine structures with optimal bond valence sums (i.e., compounds where the sums of the bond valences about each ion are close to the formal charge on the ions). Woodward et al. then used semiempirical calculations to determine some of the interactions that are important in stabilizing some of the different tilt schemes.[14] α-AlF₃ represents an interesting system for detailed investigation because, unlike the perovskites, the distortion of this material from the cubic BX₃ phase cannot be rationalized in terms of the interactions involving the A cations.

* To whom correspondence should be addressed.
† SUNY Stony Brook.
‡ University College London.
§ Oxford University.
# Present address: Department of Chemistry, Brookhaven National Laboratory, Upton, New York.
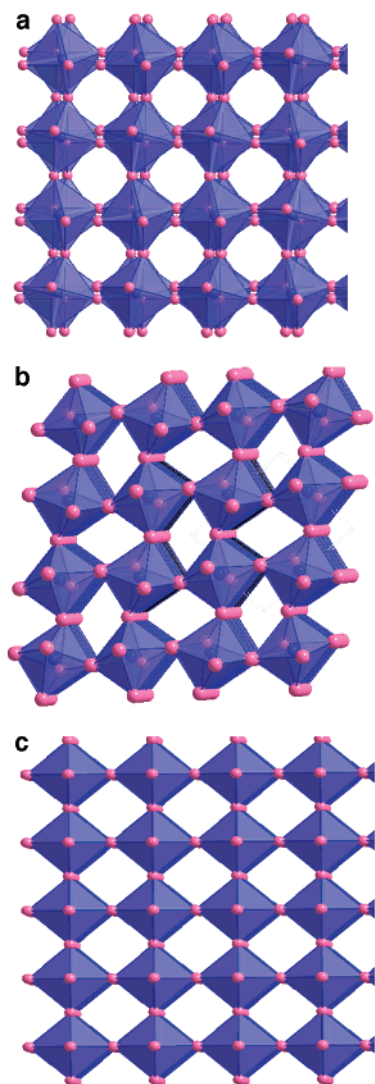⊥ Present address: Materials Science Division, Argonne National Laboratory, Argonne, Illinois.

Figure 1. (a) Rhombohedral $a^-a^-a^-$ tilt system, which contains alternate tilts of successive planes of octahedra. (b) View down the a^+ direction in the orthorhombic ($a^+b^-b^-$) form, showing the identical tilt directions of the octahedra in successive layers. (c) The cubic phase ($a^0a^0a^0$).

The introduction of polarizability terms to the description of the interactions between the B and X anions should, in theory, provide a driving force for the distortion from cubic symmetry. The first aim of the work presented in this paper is to develop a model with which to describe the distorted form of α-AlF$_3$, by using the polarizable ion model (PIM) developed by Madden and Wilson.[17] This model is then used in this paper to examine the structural variations and dynamics of the BX$_3$ octahedra that presumably result in the high-temperature phase transition to the cubic phase, as a function of temperature. Developing a model for α-AlF$_3$ that will allow the phase transition to be followed represents a challenge because a simulation cell (i.e., the collection of atoms used in the simulations) with both flexible cell lengths and cell angles is required. The model should also be designed to allow one of the longer term goals of this study to be addressed (which is not a subject of this paper), namely, to examine the effect of particle size and shape and impurities (such as O^{2-} and Cl$^-$) on the temperature dependence of the structural distortions, with a view to understanding the differences between the pure, and catalytically active materials.[6] In this paper, we use the model to investigate the

effect of temperature on the distorted AlF$_3$ phases and to investigate the types of motion that drive the high-temperature phase transition.

The α-AlF$_3$ phase adopts a rhombohedral $R\bar{3}c$ space group with cell angles $\alpha = \beta = 90°$ and $\gamma = 120°$ at room temperatures and a c parameter that is much longer than the a and b parameters (cell lengths $a = b = 4.9305$ Å and $c = 12.4462$ Å).[6] The structure comprises corner sharing AlF$_6$ octahedra with alternate tilting directions in successive planes of octahedra (Figure 1a). This tilting system is denoted as $a^-a^-a^-$ using the notation introduced by Glazer for perovskites.[11] In this scheme, the tilt systems are defined along the three orthogonal axes a, b, and c, which define the directions of the original cubic ($Pm3m$; $a^0a^0a^0$; Figure 1c) cell. The superscripts (+, 0, or −) indicate the sense of the tilt in successive layers, + and − indicating in phase (+) or out of phase (−) tilts. The letters a, b, and c are used to indicate the relative sizes of the tilts in the three orthogonal directions. For example, a tilt scheme $a^-b^-b^-$ indicates that the sizes of the tilts along the b and c axes are identical, but differ in magnitude from the size of the tilt along the a axis. The tilt scheme shown in Figure 1b, $a^+b^-b^-$, contains both different extent of tilts and arrangements of AlF$_6$ octahedra in the a and (b/c) directions.

The Al−F−Al bond angle can be used as one measure of the extent of tilting (or rhombohedral distortion), and at room temperature it ranges from 157.1 to 157.9°.[5,6] In earlier detailed Raman, X-ray diffraction, and differential scanning calorimetry (DSC) studies,[5] a first-order phase transition, with significant hysteresis, was observed at approximately 456 °C by DSC. The normal mode vibrations were followed across the phase transition to understand the nature of the dynamics. The A$_{1g}$ mode, which is Raman active in the rhombohedral phase, was proposed to be the mode associated with the rotation of the octahedra. This mode gives rise to a low-frequency resonance (158 cm^{-1}) that shifts to lower frequency and then eventually vanishes in the cubic phase (where it becomes the R$_5$ mode, which is no longer Raman active). The softening of this mode is considerable, where the authors correlating this softening with increasing anharmonicity at higher temperatures. We followed this phase transition by in situ X-ray diffraction (XRD) methods[6] for a powdered sample of α-AlF$_3$ and found that a small residual rhombohedral distortion persisted above the phase transition, Al−F−Al bond angles of 176° being observed at 500 °C. In subsequent work on single crystals[7] of α-AlF$_3$, the cubic phase was observed above the phase transition; thus, the remnants of the rhombohedral phase seen for the powder appear to be associated with either the presence of small levels of impurities in the powdered phase or possibly particle-size effects. The electron density maps[7] generated for the single crystal above the phase transition from the XRD data suggest the existence of electron density due to fluorine that does not directly lie between the two Al atoms. This electron density resulted in large anisotropic thermal ellipsoids for the fluorine atoms, when the structure was refined with the cubic structural model. Furthermore, the apparent Al−F bond lengths *decrease* with temperature, which again indicates that the F atoms are not necessarily located between the Al−Al interatomic vectors. Both sets of experimental data suggest that the high-temperature phase still contains bent Al−F−Al units but that the AlF$_6$ units rapidly rock backward and forward *or* rotate so that on average the system appears cubic. The difference between these two motional modes is similarly nontrivial to detect in the simulations, by simply tracking readily extractable parameters such as the bond angles and lengths. In addition, simple visualization

TABLE 1: Short-Range and Dispersion (Including Damping) Parameters (in Atomic Units) Used to Describe the Potential for AlF₃[a]

ion pair	a^{ij}	B^{ij}	C_6^{ij}	C_8^{ij}	b_6^{ij}	b_8^{ij}
$-$ $-$	2.164	122.77	45.337	487.894	2.9	2.9
$-$ $+$	2.200	99.50	1.0	0.0	1.9	1.0

[a] The dipole polarizability was 5.983 au, the damping parameter b_{AlF}, 1.80 au, c_{AlF}, 1.38 au and the cut-off r_c, 15.50 au.

of the process becomes particularly difficult at high temperatures where the systems are typically disordered and very dynamic. In this paper, we introduce two correlation functions which allow us to track the overall motion of the AlF₆ octahedra and analyze this motion in more detail. These approaches should prove useful diagnostics in our simulations of increasingly disordered systems (such as the nanoparticles).

In this work, we attempt to clarify the nature of the motion that leads to the observation of cubic symmetry, when the structure is probed by diffraction methods. The simulation methods are first presented, along with the methodology used or developed to analyze the results. This is followed by a detailed analysis of the results from the calculations.

2. Simulation Details

The simulations were carried out a polarizable ion model as described in detail elsewhere.[17] In this model, a Born−Mayer pair-potential of the form

$$U_{ij} = \frac{Q^i Q^j}{r_{ij}} + B_{ij}e^{-a_{ij}r_{ij}} - \sum_{n=6,8} \frac{C_{ij}^n}{r_{ij}^n} f_{ij}^n \quad (1)$$

is augmented with a description of the (many-body) ion polarization effects. $Q^{i(j)}$ are the formal (valence) ion charges of ions $i(j)$, r_{ij} is the distance between the ions (in atomic units), B_{ij} and a_{ij} control the repulsive short-range interactions, and C_{ij}^n ($n = 6$ and 8) are the dispersion coefficients for the dipole−dipole and dipole−quadrupole interactions, respectively. These parameters are determined from the ab initio ion polarizabilities extracted from electronic structure calculations (see below) using standard methods.[18−20] The dispersion terms are modified by the damping functions, f_{ij}^n to account for overlap of the ion electron densities at short range. The short-range parameter sets $\{a_{ij}, B_{ij}\}$ were obtained by optimization against the experimental bond lengths and bond angles determined for rhombohedral α-AlF₃ and the optimized parameter set is listed in Table 1.

The induced moments in the PIM are included as additional degrees of freedom using an extended Lagrangian formalism. In the present work, induced dipoles were only included on the anions since the polarizability of the Al³⁺ cation is very small ($\alpha_{Al^{3+}} = 0.265$ au[18]), and furthermore, the cations tend to sit in highly symmetric (octahedral) symmetry sites which precludes the formation of such low order moments. As a result, the minimization of the potential

$$V^{pol} = \sum_{i,j \in all \ ions} \{(Q^i\mu_\alpha^j - Q^j\mu_\alpha^i)T_\alpha^{(1)}(r_{ij})f_{ij}(r_{ij}) -$$
$$\mu_\alpha^i T_{\alpha\beta}^{(2)}(r_{ij})\mu_\beta^j\} + \sum_{i \in anions} k^i\mu^{i2} \quad (2)$$

with respect to the dipole set $\{\mu_\alpha^i\}$ (in which the cation dipoles are set to zero) for a given ion coordinate set leads to self-consistent dipoles on the anions and hence gives the overall polarization energy. The final term in the equation is a Drude-

like expression representing the energy required to polarize an ion with the force constant, k^i, related to the dipole polarizability, α^i, of the ion i by $k^i = 1/2\alpha^i$. $T_{\alpha\beta}^{(2)}$ ... are the multipole interaction tensors.[21]

In eqs 1 and 2, the functions f^n are the modified Tang−Toennies[22] damping functions of the form

$$f_{ij}^n = 1 - ce^{-br}\sum_{m=0}^n \frac{(br)^m}{m!} \quad (3)$$

which varies from 1 at large r to $(1 - c)$ at small r, with a range parameter b. This function is used to represent the short-range contributions to both the induced dipoles and dispersion interactions, as uncovered in electronic structure calculations.[19] For the dispersion interactions, a value of $c = 1$ is used corresponding to the original Tang-Toennies functions, whereas for the induced dipole damping, a value of $c = 1.38$ au is used. The use of a c parameter greater than one reflects the fact that, at short ion separations, the dipole induced by the short-range interactions may become larger than that induced by the ion charges.[19]

The polarizability of the F⁻ ion is taken as that determined by electronic structure calculation for the anion in the LiF rock-salt environment ($\alpha_{F^-} = 5.983$ au).[23] The value of b_{AlF} was generated by scaling the value calculated ab initio for LiF by the appropriate ion radii as follows:

$$b_{AlF} = b_{LiF}\frac{\sigma_{Li^+} + \sigma_{F^-}}{\sigma_{Al^{3+}} + \sigma_{F^-}} \quad (4)$$

The validity of this procedure has been verified by electronic structure calculations and has been found to be applicable both intra- and interstoichiometrically.[19]

The initial crystal was set up in a hexagonal simulation cell to correspond to the ambient temperature experimental structure for α-AlF₃.[6] The cell is comprised of 4 × 4 × 2 (for the a, b, and c directions in the noncubic simulation cell) crystallographic unit cell lengths and contains 768 atoms in total. The simulations are run under constant stress conditions by extending the constant pressure method of Andersen[24] (in the manner described by Parrinello and Rahman[25]) in which both shape and size of the simulation cell can change dynamically. We have implemented the invariant equations of motion as given by Martyna et al.[26] The ions and the barostats are both coupled to Nosé-Hoover chains of length 5. All long-range interactions (up to terms which vary with interionic separation as r^{-4}) are described by the Ewald method, adapted to noncubic cells as described by Nosé and Klein.[27] A fixed spherical cutoff at r_c is imposed on the interactions in real-space. An Ewald convergence parameter η is chosen such that $\eta r_c = 5.6$.[28] The number of k vectors in the reciprocal space sum was varied as the cell shape changed so as to ensure convergence.

The trajectory (atomic coordinates and velocities) was stored every 10 steps. These stored data were then analyzed in more detail at the end of each run, as described in the next section. Temperature ramps were performed by increasing the temperature and running the simulations for 10 ps in order to stabilize the system at the desired temperature. The final output data file was then used as the initial input file for a longer MD run (typically 100 ps), performed to analyze the dynamics at the new temperature. Nosé-Hoover thermostat relaxation parameters of 1 ps were used in the temperature ramp, whereas a much larger value of 10 ps was used for the constant temperature simulations.

3440 *J. Phys. Chem. B, Vol. 108, No. 11, 2004*

Chaudhuri et al.

3. Analysis Methods

The radial distribution functions (rdfs), $g_{Al-Al}(r)$, $g_{Al-F}(r)$, and $g_{F-F}(r)$, were calculated in order to determine the bond length distributions and give insight into the relative disorder in each coordination sphere. Bond angle distributions (BADs) were calculated for the Al−F−Al triplets with two Al−F bond lengths that are shorter than or equal to the position of the first minimum in $g_{AlF}(r)$. Information regarding this particular triplet is especially useful since the fluoride ions sit at the corners of the AlF_6 octahedra and are shared by pairs of Al^{3+} cations (which sit in the centers of the octahedra). As a result, the Al−F−Al BAD contains information relating to the relative tilt orientations of neighboring octahedra.

Simulation models offer a level of data (such as atom positions and velocities) which are not largely directly accessible to the experimentalist. However, because of thermal and other sources of disorder, the crystal structure may be difficult to assign for a particular configuration set. As a result, the effective powder diffraction pattern is calculated from the simulation cell and compared to the experimentally determined patterns. The partial structure factors are calculated directly at every molecular dynamics time-step

$$S_{\alpha\beta}(k) = A_\alpha(k)A_\beta^*(k) \tag{5}$$

where $A_\alpha(k)$ is the scattering amplitude of species α given by

$$A_\alpha(k) = \frac{1}{\sqrt{N_\alpha}}\sum_{i=1}^{N_\alpha} e^{i\mathbf{k}\cdot\mathbf{r}_i} \tag{6}$$

The scattering vectors $\mathbf{k}$ are the reciprocal lattice vectors of the periodically replicated simulation system at the time-step of interest. The "powder" pattern is obtained by averaging over scattering vectors of equal length.

For crystalline systems, the structure factors consist of a series of well-defined Bragg peaks. The X-ray total structure factor, $F^{(X)}(k)$, can then be constructed from the three partial functions

$$F^{(X)}(k) =$$
$$[f_{Al}(k)^2 c_{Al}[S_{AlAl}(k) - 1] + 2f_F(k)f_{Al}(k)\sqrt{c_F c_{Al}}S_{AlF}(k) +$$
$$f_F(k)^2 c_F[S_{FF}(k) - 1]]/[f_{Al}(k)^2 c_{Al} + f_F(k)^2 c_F] \tag{7}$$

where $f_\alpha(k)$ is the k-dependent X-ray form factor and c_α is the mole fraction of species α. The form factors for the Al^{3+} and F^- ions are taken from standard sources.[29]

We have introduced two correlation functions to characterize the time evolution of the relative tilt of adjacent coordination polyhedra. For a given pair of Al^{3+} ions, k and l, we identify the F^- ion that bridges between them as the one which is within a given distance (first minimum of g_{AlF}) of both Al^{3+} ions. The midpoint of the line joining the two Al^{3+} ions (which corresponds to the F^- position in the perfect ReO_3 structure, Figure 2), $\mathbf{r}_c$ is

$$\mathbf{r}_c = (\mathbf{r}_k - \mathbf{r}_l)/2 + \mathbf{r}_l \tag{8}$$

and the displacement of the F^- ion, i, from this position is

$$\delta_i = \mathbf{r}_i - \mathbf{r}_c \tag{9}$$

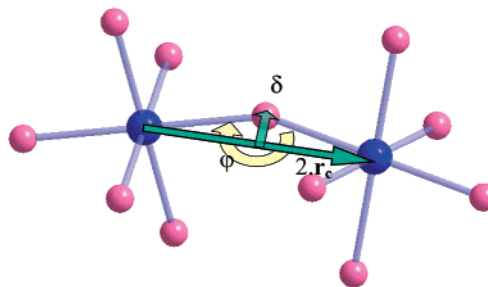We then calculate the time correlation function (averaged over all fluoride ion displacements)

Figure 2. Vectors used to monitor the motion of atoms. The value of the experimental Al−F−Al angle φ in the rhombohedral phase is 157.9°. The displacement vector δ represents the vector drawn from midpoint of $\mathbf{r}_{Al-Al}$ ($\mathbf{r}_c$) to the fluoride atom's instantaneous position $\mathbf{r}_i$.

$$C_{disp}(t) = \langle|\delta_i(t)||\delta_i(0)|\rangle \tag{10}$$

which will examine the size of the deviation of the F^- ions from the perfect ReO_3 position and which will relax to a finite value if the Al−F−Al bond angle differs from 180°. We can also calculate

$$C_{angle}(t) = \langle\hat{\delta}_i(t)\cdot\hat{\delta}_i(0)\rangle = \cos(\theta_i(t)) \tag{11}$$

where $\hat{\delta}_i$ is a unit vector formed from $\delta_i(t)$ and $\theta_i(t)$ measures the angle between the displacement of i at time t and at the initial time. If the direction of tilt of two adjacent polyhedra does not change (as in the rhombohedral structure), $C_{angle}(t)$ will relax to a finite value, whereas if the direction of tilt precesses freely it will relax to zero.

4. Results

4.1. Validation of the Model and Analysis of the Structure. A comparison of the bond lengths and cell lengths with those of the experimental crystallographic structure was first carried out with the simulation cell obtained at 400 K to test the accuracy of our potential model. The Al−F−Al bond angle and, thus, the degree of tilting is similar to that found experimentally (157° compared to 157.1° or 157.9°)[5,6] at close to room temperature, whereas the average Al−F bond distance (1.78 Å) is very slightly shorter than that found experimentally (1.797 Å). In view of this reasonable agreement, the system was then heated to 900 K, in steps of 50 K, and then cooled back to 400 K, in 100 K steps, to examine the effect of temperature on the structure and dynamics of the system. Simulations were run for time intervals of 100 ps or more at each temperature step.

The AlF_6 units are rigid at room temperature rocking or vibrating only slightly about their center of masses. As the temperature is increased, the amplitude of the rocking motion increases steadily. The bond-angle distribution obtained from the simulations for each temperature run is shown in Figure 3. Surprisingly, the bond angle decreases very slightly on heating from 400 to 500 K. The bond-angle then increases noticeably, from a median angle of approximately 156° at 500 K to close to 180° at high temperatures, as the simulation temperature is raised. A clear discontinuity in the bond-angle distribution is observed between 600 and 650 K: At 600 K, a broad maximum is seen at approximately 166°, whereas above this temperature, the broad distribution is centered at 180°; we ascribe this change to the high-temperature phase transition of α-AlF_3. Thus, within the limit of our accuracy of the temperature steps (50 K), this transition occurs between 600 and 650 K. The broad distribution of bond angles above the phase transition suggests that most of the Al−F−Al bonds are bent, even in the high-temperature phase.
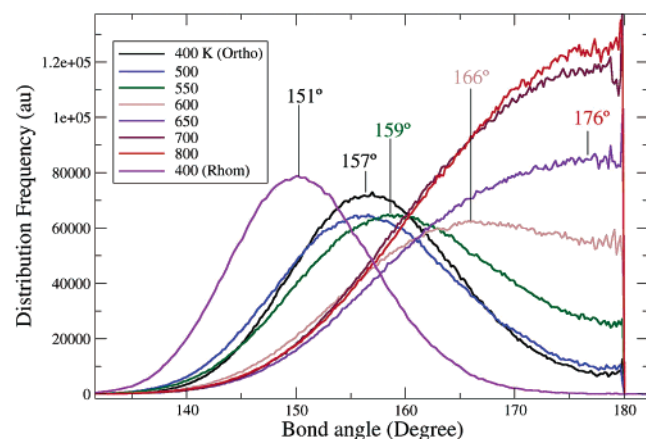
Figure 3. Bond angle distribution as a function of temperature. Two distributions are shown for 400 K, where 400 K (Ortho) is the initial structure model, whereas 400 K (Rhom) corresponds to the structure obtained by cooling the 500K rhombohedral phase.
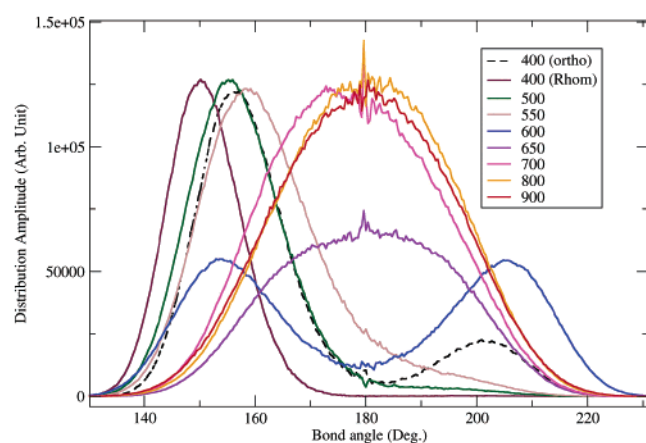

Figure 4. Cross-product modified bond-angle distribution plot showing the difference between the tilting schemes in the two 400 K and the higher temperature phases.

1. Modified Bond Angle Distribution. The bond angle distributions described above, although informative, do not provide any information concerning the relative orientations of the Al−F−Al linkages (and thus the sense of the octahedral tilts), since all of the bond angles are less than 180° regardless of the spatial orientation of the two bonds. Furthermore, these plots cannot be used to determine whether a change in the direction of the tilt of the octahedra has occurred during the course of the run. To access this information, we introduced a refinement to the standard bond angle distribution calculation. The two Al−F bonds, which share a central F$^-$ anion and form a Al−F−Al triplet, can be defined by the vectors r_1 and r_2, where $r_1 = r_{Al,1} - r_F$ and $r_2 = r_{Al,2} - r_F$. The cross product of these two vectors, $r_1 \times r_2$, results in a single vector whose orientation contains the information regarding the orientation of the Al−F−Al triplet. By taking the scalar product of this cross product with a given reference vector, r_{ref}, we can classify each Al−F−Al bond angle as either being less than or greater than 180°. By choosing r_{ref} to be the initial hexagonal cell vector, *a*, we dictate that all of these modified bond angles, φ, are < 180°, in the rhombohedral ($a^-a^-a^-$) AlF$_3$ structure.

Two peaks are now observed in the modified bond-angle-distribution at 157 and 202° at 400 K (Figure 4), with the peak at 157° being noticeably larger than the one at 202°. The presence of two peaks indicates that the sense of octahedron tilting is not the same for all of the Al−F−Al linkages, as only

one peak at <180° is predicted for the rhombohedral, $a^-a^-a^-$ AlF$_3$ structure. As the temperature is increased to 500 K, the maxima in φ above 180° disappears, indicating that a change in the sense of octahedra tilting has occurred. The maximum in φ shifts to higher angles at 550 K, but the tilting scheme remains similar. At 600 K, however, the distribution changes again, and two equal maxima for φ are observed at $180 \pm 26°$. Given the symmetry and three-dimensional connectivity of the AlF$_6$ octahedra, it is not possible to generate a single tilting scheme that generates an equal probability for the two tilt directions. This distribution can, however, be explained by the onset of a motion that results in an averaging of the sense of the tilt direction during the course of the MD run. The nature of this motion will be explored in more detail in the correlation function analysis section presented later. At higher temperatures, the maximum in φ is seen at approximately 180°, and the distribution is centered about this angle. These plots suggest that the tilting angles and the tilting schemes of the octahedra do not remain constant as the temperature is increased. Furthermore, significant changes in the arrangements of the octahedra occur at temperatures well below the high temperature phase transition at approximately 600−650 K.

Clearly, our system cannot be described based simply on the tilting schemes described earlier for α-AlF$_3$. More detailed examination of the 400 K simulation cell revealed that the tilting scheme differs in one direction from that of the experimental structure (Figure 5a snapshot of 400 K structure). The tilting schemes in the other two orthogonal directions are the same as those found in the $R\bar{3}c$ structure. The Glazer notation for this tilting scheme is either $a^+b^-b^-$ or $a^+a^-a^-$ (tilt system nos. 10 and 11), which both give rise to structures that adopt the orthorhombic space group *Pnma* (see Figure 1b). We will use the label $a^+b^-b^-$ throughout this paper to indicate that the tilt angles for the two types of tilts are not necessarily the same in our system. This tilt system is one of the more common tilts adopted by the ABX$_3$ perovskites and is consistent with the observation of a peak at $\varphi = 202°$ ($360° - \varphi = 158°$) at 400 K in the cross-product modified bond angle distribution plot corresponding to the a^+ direction of the tilt scheme.

The $a^+b^-b^-$ phase is no longer stable at 500 K and transforms to a new phase with the $a^-a^-a^-$ tilting scheme, accounting for the change in the number of peaks in the cross-product modified bond angle distribution plot between 400 and 500 K *and* the very slight decrease in the Al−F−Al bond angle to approximately 156°. Although the 500 K structure is more disordered than the 400 K one, largely due to the increased motion, snapshots of the structure (Figure 5b) clearly show the alternating tilts of the octahedra, down the *a*, *b*, or *c* axes. The rhombohedral phase is stable up to approximately 600 K, where the onset of a second phase transition is observed. Based on Figure 5, where values of $\varphi = 180 \pm 26°$ are seen, the AlF$_6$ octahedra are still tilted in this phase, but distributed evenly on either side of the Al−Al vectors. This can be seen in the snapshot presented in Figure 5c.

The high-temperature phase transition is reversible, the system returning on cooling to 500 K to a cell with similar bond angles and cell parameters to that observed on heating. Further cooling to 400 K does not, however, result in a change in the tilt system even for extended MD runs. The $a^-a^-a^-$ tilt system remains, but the average Al−F−Al bond angle drops to approximately 151°. The energies of the two 400 K phases are very similar, and presumably, the activation energy associated with the reordering of the octahedra tilting is too high and the thermo-
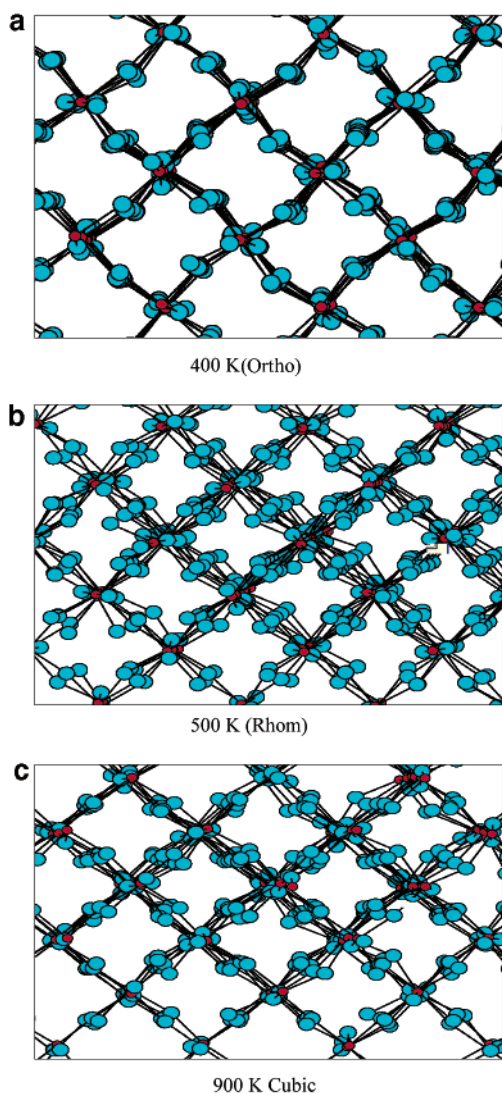
3442 *J. Phys. Chem. B, Vol. 108, No. 11, 2004*

Chaudhuri et al.

Figure 5. Snapshots of the α-AlF$_3$ 400 K orthorhombic phase (a), 500 K rhombohedral phase (b), and the 650 K phase (c), showing the differences in the tilting of the AlF$_6$ octahedra.

dynamic driving force is not sufficient to convert the $a^-a^-a^-$ to the $a^+b^-b^-$ phase, at least within the time period of the MD run.

2. Partial Radial Distribution Functions and Cell Parameters. The partial rdfs for the Al−F and Al−Al pairs, calculated for α-AlF$_3$ from 400 to 900 K, are shown in Figure 6. The first peak at 1.78 Å in the $g_{Al-F}(r)$ plot corresponds to the average Al−F bond length. This peak does not split or show any asymmetry as a function of time and temperature indicating that the average Al−F bond length remains constant throughout. The peak does, however, broaden as the Al−F bonds undergo thermal vibrations with increasing amplitudes around their mean bond length, with increasing temperature. The next set of peaks at approximately 4 Å, which correspond to distances between Al atoms and F atoms in connected octahedra, are split at 400 K, two peaks being observed at approximately 3.7 and 4.2 Å for the orthorhombic phase, as a result of the tilting of the corner shared octahedra (see Figure 2a). The peaks broaden noticeably at 600 K. A discrete change is seen at the high-temperature phase transition and at 650 K, and above a single, very broad peak is observed indicating that there is still a large distribution in distances, consistent with considerable motion of the octahedra in the cubic phase.
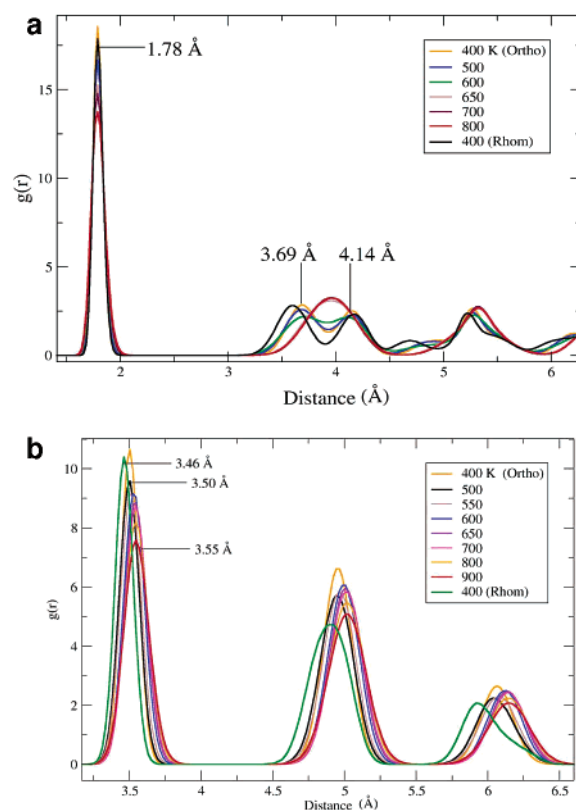

Figure 6. Partial radial distribution function (rdf) plots:(a) Al−F rdfs; (b) Al−Al rdfs.

The peak corresponding to the nearest Al−Al distances (i.e., Al atoms in connected octahedra) gradually shifts to larger values in the Al−Al rdf plot (Figure 6b) as the temperature increases from 400 to 900 K. The slight asymmetry in the rdf peak shape indicates that the Al−Al distances are slightly different along the three (close-to) orthogonal Al−F−Al chains. The low-temperature rhombohedral phase Al−Al distances, obtained on cooling to 400 K, are slightly shorter (3.46 Å) than the 400K $a^+b^-b^-$ form (3.50 Å), consistent with the smaller Al−F−Al bond angle seen for this phase.

Although the space group of the room temperature $a^+b^-b^-$ phase is clearly no longer rhombohedral, we can still define a pseudo-rhombohedral cell with cell-edge vectors corresponding to those of the overall simulation cell and with a, b, and c parameters close to those of the original rhombohedral cell (determined by dividing those of the simulation cell by 4, 4, and 2 for the a, b, and c directions, respectively). This allows us to compare the extent of tilting in the different cells, independent of the tilt system. The volume of the simulated cell drops (Figure 7) slightly from 400 to 500 K, due to the smaller Al−F−Al bond angles of the rhombohedral phase. The volume then increases steadily as the temperature is increased further, leveling off above the rhombohedral-to-cubic phase transition. The simulated and experimental cell-volumes are compared in Figure 7.

3. Simulated X-ray Diffraction Patterns. The total X-ray scattering factors were calculated as described in section 3, to follow the crystal symmetries of the low and high temperature structures and to provide output that can be directly compared with experimental data or with X-ray diffraction patterns calculated using different structural models. In addition, it is useful to validate such procedures for the bulk crystals since we anticipate that they will be particularly helpful for our studies of the AlF$_3$ nanocrystals.
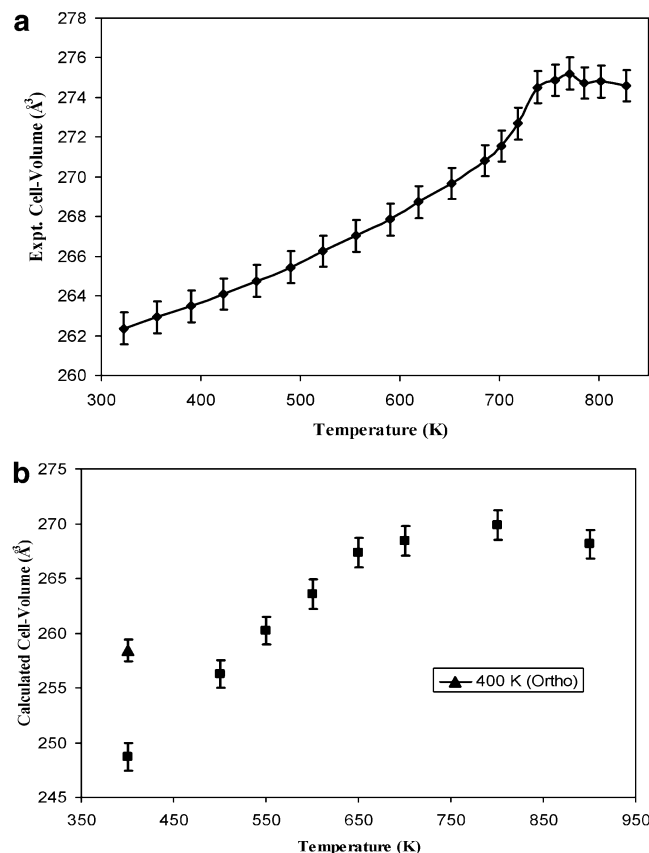
Figure 7. Cell volume obtained (a) experimentally from in situ time-resolved synchrotron X-ray diffraction data[6] and (b) from the simulations at different temperatures.
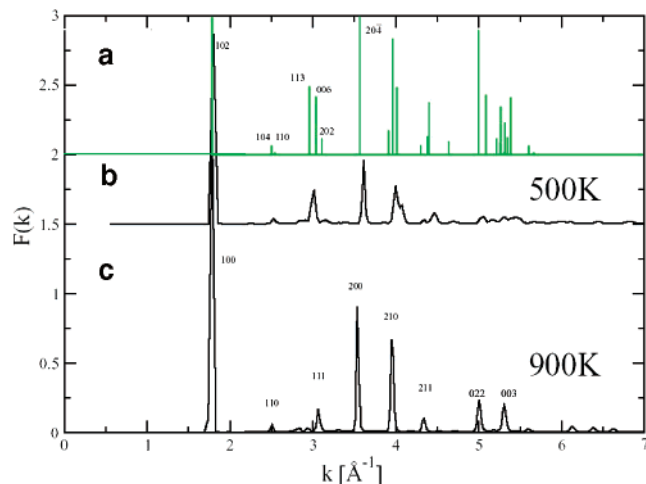

Figure 8. Comparison of the X-ray diffraction powder pattern obtained from the 500 K simulations (a) and the X-ray powder pattern calculated for a rhombohedral structure (b), with cell parameters of 5.003 and 11.95 Å, for a and c, respectively, and Al and F atoms at (0, 0, 0) and (0.42, 0, 0.25),[6] respectively. (c) The calculated X-ray diffraction pattern for the high-temperature phase obtained from the 900 K simulation data.

Figure 8 shows the total X-ray scattering factors obtained from the calculated partial structure factors using eq 7 at 500 and 900 K. In both cases, the diffraction patterns are calculated over 60 ps of ion dynamics. The calculated X-ray powder pattern for the ideal rhombohedral structure is shown in the same figure for comparison. This pattern was calculated by setting the length of the unit cell along the *a* direction to be equivalent to that in the *b* direction, by calculating the mean of the *a* and *b* unit cell
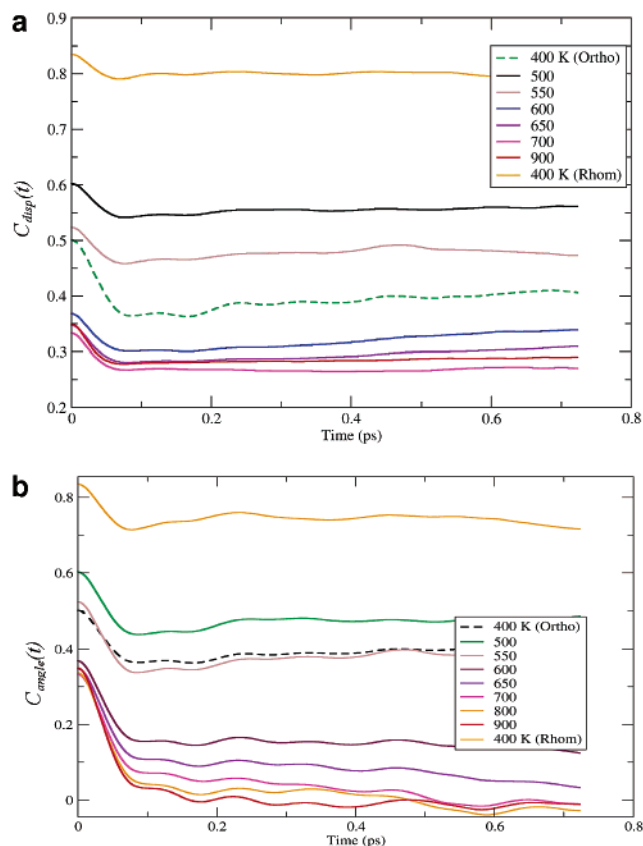

Figure 9. Time correlation function plots used to follow the motion of the Al−F−Al linkages. (a) The displacement-time correlation function, which tracks the change in the average distance of the F atom from the position of a F atom in a hypothetical linear Al−F−Al linkage and (b) the angle-time correlation function, showing the angular correlation between the Al−Al and Al−F vectors.

dimensions during the simulation run for the 500 K system ($a \equiv b = 4.79$ Å). The *c* length is determined from the mean of the fluctuating *c* unit cell length ($c = 11.94$ Å). For the cubic unit cell, the ideal scattering function is calculated with a single mean unit cell length determined from the fluctuating cell lengths from the simulation at 900 K.

The major peaks observed in the calculated total X-ray scattering factor, for the system at 900 K, can be indexed to a cubic $Pm\bar{3}m$ unit cell. Three weaker peaks are present at 2.8, 2.9, and 3.3 Å⁻¹. The peaks at 2.8 and 3.3 Å⁻¹ can be indexed to the 310 and 321 reflections from a lower symmetry, $Im\bar{3}$ cubic cell derived by a rotation of the octahedra about all three axes, with identical tilting schemes in successive layers of tilted octahedra ($a^+a^+a^+$ in the Glazer notation). This alternate tilting scheme results in a doubling of the cell parameters in all three directions. These reflections contain information about the fluorine positions only, and are systematically absent for a^- or a^0 tilts.[31,32] This suggests that these additional peaks arise from the finite time intervals during the simulation run where the tilted chains of octahedra are oriented in the same direction in adjacent layers. We note, however, that the $Im\bar{3}$ cell contains additional weaker reflections that are not observed in our pattern obtained from the MD simulations, the intensities of all of these reflections depending strongly on the fluoride ions positions. The simulated total diffraction pattern for the system at 500 K closely matches the calculated pattern.

4.2. Ion Dynamics. The time correlation functions are plotted in Figure 9 to probe the dynamics responsible for the phase transition in more detail. The perpendicular component of

motion, δ, decreases with time but then levels off at a fixed positive value at all temperatures. The value of δ at longer times is smaller for the 400 K orthorhombic phase than for the 400 K rhombohedral phase, consistent with the smaller average Al–F–Al bond angle for the rhombohedral phase. The correlation function value of $C_{disp}(t)$ for the rhombohedral phase decreases as the temperature is raised, dropping noticeably at the phase transition (to approximately 0.42 Å^2), where it remains essentially constant as the temperature is raised further. Thus, even in the high-temperature phase where there is considerable motion, this motion does not, for the majority of fluoride ions, involve librational modes where linear Al–F–Al linkages are formed. Figure 9b shows the angle correlation function, $C_{angle}(t)$. The correlation function drops steadily as the temperature of the rhombohedral phase is raised, consistent with a steady increase in the amplitude of the motion of the AlF$_6$ octahedra about the Al–Al axis. Different behavior is seen above the high-temperature phase transition temperature, where $C_{angle}(t)$ drops steadily to zero, indicating that the motion in the system now involves complete reorientations of the octahedra (i.e., a reverse in the sense of tilting of the octahedra).

The high temperature phase is distinguished from the rhombohedral phase by the constantly varying tilt directions of the octahedra during the MD run. In theory, the change in tilt direction can be achieved via two mechanisms. The first involves a cooperative rotation of the connected octahedra in an Al–F–Al chain about the Al–Al bond vector, $2r_c$ (as indicated by a curved arrow in Figure 2), whereas the second involves a cooperative flip of all of the connected AlF$_6$ octahedra in a Al–F–Al chain, the fluoride ions crossing directly through the Al–Al interatomic vector, midway through the jump process. The combination of a nonzero distance correlation function $C_{disp}(t)$ and a zero angular correlation function $C_{angle}(t)$ indicates that the first mechanism predominates, since a passage of a fluoride ions through the Al–Al vector would result in a zero value of δ. A contribution from the second mechanism cannot be completely ruled out for a small subset of fluoride ions as the bond angle distribution plot indicate that some of the Al–F–Al linkages are close to linear at higher temperatures. The presence of some close-to-linear linkages is not too surprising, however, due to increased amplitude of all of the vibrational modes at higher temperatures. These large vibrations of the AlF$_6$ octahedra may couple with the rotational motion to help lower the activation energy for the cooperative rotation of the chains.

5. Discussion

Both the $a^-a^-a^-$ and $a^+b^-b^-$ tilt systems are commonly observed for perovskites with only one type of A cation and the energies of both forms are similar. Woodward et al[14] showed, using semiempirical calculations, that the $a^-a^-a^-$ tilt is favored in systems with small repulsion terms, whereas the $a^+b^-b^-$ tilt system strikes an optimum balance between maximizing Coulombic attractions and minimizing the anion–anion repulsions. Since the final form adopted is a delicate balance between a number of terms, it seems likely that the final result will show a dependence upon the empirical potential used. Since there are no A cations in the BX$_3$ systems, the polarization of the anion charge cloud is likely to play a larger role in dictating the structure type. The $a^+b^-b^-$ should still be favored over the $a^-a^-a^-$ structure based on anion repulsion terms, but for systems with similar bond angles, however, the $a^-a^-a^-$ system should be favored based on the dipole terms. As the Al–F–Al bond bends, the F$^-$ electron density cloud will distort, so as to move toward the center of the Al–Al interatomic vector. This serves
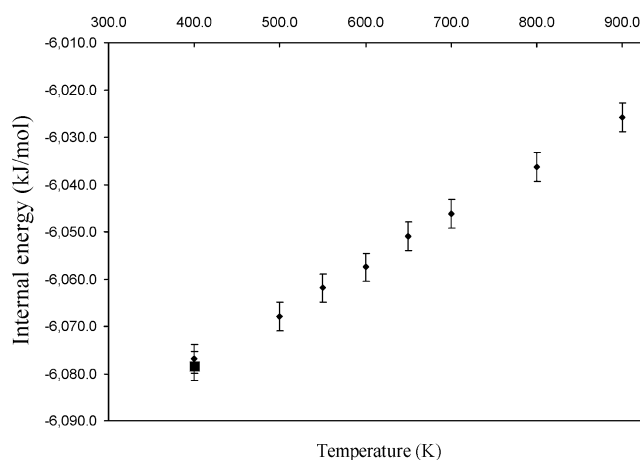

Figure 10. Change in the average internal energy with temperature.

to reduce both the Al–Al and F–F repulsion terms with respect to the valence charge-only repulsions. Dipole–dipole repulsions are minimized by arranging the F$^-$ dipoles in opposite directions both along the Al–F–Al chains and from layer to layer, as occurs in all three directions in the $a^-a^-a^-$ structure but only in two directions in the $a^+b^-b^-$ tilting scheme. Thus, $a^-a^-a^-$ represents the optimum arrangement for the dipoles, providing one explanation for the smaller Al–F–Al bond angles (and, therefore, larger dipoles) in this phase, in comparison to $a^+b^-b^-$ phase.

The total internal energy (Figure 10) of the simulation cell in the 400 K rhombohedral form is -6078.4 kJ mol^{-1}, which is very similar to that of the orthorhombic form (-6076.8 kJ mol^{-1}). The contribution to the total energy from the polarization (as given by the term in μ^2 in eq 2) is quite different for the two forms, the rhombohedral form having a higher value (30.1 kJ mol^{-1}) in comparison to that of the orthorhombic form (23.2 kJ mol^{-1}). The dipole moment at the fluoride ions increases as the Al–F–Al bond angle decreases from linear. As a result, the smaller bond angles in the room-temperature rhombohedral phase will result in a larger value for the polarization energy. The smaller polarization contribution to the total energy of the orthorhombic phase may be compensated by other physical terms such as a smaller F–F repulsion. The small energy difference between these two phases may be attributed to the smaller average Al–F–Al bond angle in the rhombohedral structure.

The higher symmetry $a^-a^-a^-$ phase should become increasingly more stable in comparison to the orthorhombic phase at higher temperatures due to the higher entropy of this phase. Out-of-phase octahedral motion in each successive layer should be possible in this phase without symmetry-breaking but not in the $a^+b^-b^-$ phase. Conversely, the $a^+b^-b^-$ phase should become increasingly more energetically favorable at lower temperatures. The orthorhombic form was presumably stabilized in our simulations, because the optimization of our potential model was performed at lower temperatures where a metastable energy minimum was identified. The orthorhombic phase was only able to transform to the experimentally observed rhombohedral form at 500 K, on the time scale of our simulations. Cooling down the 500 K form to lower temperature results in a more rhombohedrally distorted phase, consistent with the potential model's slight preference for the rhombohedral form. The results suggest that the orthorhombic metastable phase will only be stable at low temperatures and that it will only be possible to prepare this phase at ambient pressures via a low-temperature synthetic route. The application of increased pressure to the

cubic (*Pm3m*) ReO₃ phase results in successive transformations of the cubic phase to a cubic *Im*3, a rhombohedral, and finally a second rhombohedral phase at approximately 40 GPa.[31,32] A monoclinic phase was also identified in one study.[31] This suggests that pressure will dramatically alter the stability ranges of the different phases identified in this study. Both experimental (diffraction) and simulations are in progress to test this hypothesis.

Finally, the heat capacity of the different phases was estimated from the gradient of the internal energy versus temperature (Figure 10), to provide estimates for the energies of the cubic and rhombohedral phases at 700 K. From an estimate of the heat capacity of the rhombohedral form ($\sim$78 J mol^{-1} K^{-1}) an energy difference of $\sim$500 J mol^{-1} is extracted, which is in surprisingly good agreement with the experimental value of 597.4 J mol^{-1}.[5]

6. Conclusions

A potential model has been developed in this paper, which is able to describe the change in structure of α-AlF₃ with temperature. The model contains a full description of the (many-body) anion dipole polarization. Unlike the case for the structurally related perovskite ABO₃ systems, where the extent and type of octahedral tilting can often be rationalized in terms of the relative sizes of the A and B cations, the anion polarization term represents the driving force for the tilts in the AlX₃ structure, and its inclusion into the potential model is clearly essential. Two polymorphs are identified in the simulations at ambient temperatures that differ in the tilting of the AlF₆ octahedra in adjacent planes. The rhombohedral phase is observed experimentally, whereas the orthorhombic phase has not been observed, but is commonly observed in perovskite materials. The rhombohedral polymorph, which is associated with larger Al−F−Al bond angles than those found in the orthorhombic phase, contains a larger contribution from the anion polarization term to the total energy, highlighting the importance of the anion polarization term in predicting the structure. The potential model is able to reproduce the experimentally observed, high temperature, rhombohedral-to-cubic phase transition, from a distorted to cubic-ReO₃ structure. The motions of the AlF₆ octahedra were investigated by monitoring specific time correlation functions that track the Al−F−Al bond angle and rotation of the octahedra about the vector connecting Al atoms in two connected octahedra. Although the median Al−F−Al bond angle increases with temperature, the simulations show that the high temperature "cubic" phase still contains tilted AlF₆ octahedra, and a snapshot of the structure does not have cubic symmetry. However, the octahedra rotate rapidly (on the time frame of an MD run) about the Al−Al vectors, so that a time-averaged representation of the structure appears cubic. The symmetries of the rhombohedral and high-temperature simulated phases have been confirmed by comparing the diffraction patterns calculated from our simulations and from the experimentally determined structure.

Our potential model is currently being used to investigate the effect of impurities and particle size on the rhombohedral distortions and surface structures in AlF₃ and related classes of materials, factors which may affect the extent of the octahedral tilts and the temperature dependences of the structures of these materials.

References and Notes

(1) McVicker, G. B.; Kim, C. J.; Eggert, J. J. *J. Catal.* **1983**, *80*, 315.
(2) DeCanio, E. C.; Bruno, J. W.; Nero, V. P.; Edward, J. C. *J. Catal.* **1993**, *140*, 84.
(3) Kemnitz, E.; Menz D. H.; *Prog. Solid State Chem.* **1998**, *26* (2), 97−153.
(4) Herron, N.; Farneth, W. E. *Adv. Mater.* **1996**, *8*, 956.
(5) Daniel, P.; Bulou, A.; Rousseau, M.; Nouet, J.; Fourquete, J. L.; Leblanc, L.; Burriel, R. *J. Phys.: Cond. Mater.* **1990**, *2* (26), 5663.
(6) Chupas, P. J.; Ciraolo, M. F.; Hanson, J. C.; Grey C. P. *J. Am. Chem. Soc.* **2001**, *123*, 1694−1702.
(7) Chupas, P. J.; Chaudhuri, S.; Hanson, J. C.; Qiu, X.; Lee, P. L.; Shastri, S. D.; Billinge, S. J. L. Grey C. P. submitted.
(8) Yang, H. X.; Ghose, S.; Hatch, D. M. *Phys. Chem. Min.* **1993**, *19*, 528.
(9) Street, J. N.; Wood, I. G.; Knight, K. S.; Price, G. D. *J. Phys: Cond. Mater.* **1997**, 647.
(10) Zhao, Y. S.; Weidner, D. J.; Parise, J. B.; Cox, D. E. *Phys. Earth Planet In.* **1993**, *76* (1−2), 1−16 and 17−34.
(11) Glazer, A. M. *Acta Crystallogr.* **1972**, *B28*, 3384.
(12) Woodward, P. M. *J. Appl. Crystallogr.* **1997**, *30*, 206−207.
(13) Woodward, P. M. *Acta Crystallogr.* **1997**, *B53*, 32−43.
(14) Woodward, P. M. *Acta Crystallogr.* **1997**, *B53*, 44−66.
(15) Lufaso, M. W.; Woodward, P. M. *Acta Crystallogr.* **2001**, *B57*, 725−738.
(16) Brown, I. D. *Structure and Bonding in Crystals*; Keeffe, M. O., Navrotsky, A., Eds.; Academic Press, New York, 1981; Vol. 2, pp 1−30.
(17) Madden, P. A.; Wilson, M. *Chem. Soc. Rev.* **1996**, *25*, 339.
(18) Pyper, N. C. *Adv. Solid State Chem.* **1991**, *2*, 223.
(19) Jëmmer, P.; Fowler, P. W.; Wilson, M.; Madden, P. A. *J. Chem. Phys.* **1999**, *111*, 2038. Domene, C.; Fowler, P. W.; Madden, P. A.; Wilson, M.; Wheatley, R. J. *Chem. Phys. Lett.* **1999**, *314*, 158. Domene, C.; Fowler, P. W.; Madden, P. A.; Wilson, M.; Wheatley, R. J. *Chem. Phys. Lett.* **2001**, *333*, 403. Domene, C.; Fowler, P. W.; Madden, P. A.; Wilson, M. *Mol. Phys.* **2002**, *100*, 3847.
(20) Fowler, P. W.; Madden, P. A. *Mol. Phys.* **1983**, *49*, 913. Fowler, P. W.; Madden, P. A. *J. Phys. Chem.* **1985**, *89*, 2581. Fowler, P. W.; Tole, P. *Mol. Phys.* **1990**, *86*, 1019. Kelly, H. M.; Fowler, P. W. *Mol. Phys.* **1993**, *80*, 135. Fowler, P. W.; Madden, P. A. *Phys. Rev. B*, **1984**, *30*, 6131. Fowler, P. W.; Pyper, N. C. *Proc. R. Soc. London A* **1985**, *398*, 377. Fowler, P. W. *Mol. Simul.* **1990**, *4*, 320.
(21) Buckingham, A. D. *Adv. Chem. Phys.* **1967**, *9*, 107.
(22) Tang, K. T.; Toennies, *J. Chem. Phys.* **1984**, *80*, 3726.
(23) Fowler, P. W.; Madden, P. A. *Phys. Rev. B* **1985**, *31*, 5443.
(24) Andersen, H. C. *J. Chem. Phys.* **1980**, *72* (4), 2384.
(25) Parrinello, M.; Rahman, A. *Phys. Rev. Lett.* **1980**, *45*, 1196.
(26) Martyna, G. J.; Tobias, D. J.; Klein, M. L. *J. Chem. Phys.* **1994**, *101*, 4177.
(27) Nosé, S.; Klein, M. L. *Mol. Phys.* **1983**, *50*, 1055.
(28) Sangster, M. J. L.; Dixon, M. *Adv. Phys.* **1976**, *23*, 247.
(29) Cromer, D.T.; Waber, J.T. *International tables for X-ray Crystallography*; Ibers, J. A., Hamilton, W. C., Eds.; Kynoch Press: Birmingham, 1974; p 71.
(30) Sowa, H.; Ahsbahs, H. *Acta Crystallogr. B* **1998**, *54*, 578.
(31) Jørgensen, J.-E.; Staun Olsen, J.; Gerwald, L. *J. Appl. Crystallogr.* **2000**, *33*, 279.
(32) Suzuki, E.; Kobayashi, Y.; Endo, S.; Kikegawa, T. *J. Phys.: Condens. Mater.* **2002**, *14*, 10589.